Evaluation of Apoptosis with ^{99m}Tc-rhAnnexin V-128 and Inflammation with ^{18}F-FDG in a Low-Dose Irradiation Model of Atherosclerosis in Apolipoprotein E–Deficient Mice

Maryam Kamkar[1], Lihui Wei[2], Chantal Gaudet[1], Michelle Bugden[3], Julia Petryk[1], Yin Duan[2], Heather M. Wyatt[3], R. Glenn Wells[1], Yves L. Marcel[1], Nicholas D. Priest[3], Ronald E.J. Mitchel[3], and Terrence D. Ruddy[1]

[1]Division of Cardiology, University of Ottawa Heart Institute, Ottawa, Canada; [2]Nordion, Inc., Kanata, Canada; and [3]Radiological Protection Research and Instrumentation Branch, Canadian Nuclear Laboratories, Chalk River, Canada

Low-dose radiation in apolipoprotein E–deficient (ApoE$^{-/-}$) mice has a protective effect with less subsequent atherosclerosis. Inflammation and apoptosis play major roles in the development of atherosclerosis. We evaluated the temporal pattern of the development of histologic atherosclerosis, inflammation with ^{18}F-FDG, and apoptosis with ^{99m}Tc-rhAnnexin V-128 at 3 time points. **Methods:** ApoE$^{-/-}$ mice were fed a high-fat diet, exposed to low-dose ^{60}Co γ-radiation of 25 mGy at 2 mo of age, and evaluated within 1 wk (2-mo group), 1 mo (3-mo group), and 2 mo (4-mo group) from the time of radiation. Mice were divided into 3 subgroups and each received ^{18}F-FDG, ^{99m}Tc-rhAnnexin V-128, or no radiotracer for autoradiography. Mice underwent euthanasia and aortic root dissection. The extent of atherosclerosis was determined by en face and Oil red O imaging. Aortic arch inflammation (^{18}F-FDG) and apoptosis (^{99m}Tc-rhAnnexin V-128) were determined with digital autoradiography. Aortic sinus sections were stained with Sudan IV for assessment of lesion area and stage, antiCD68 antibody for inflammation and anti–cleaved-caspase 3 antibody for apoptosis. **Results:** The extent of aortic atherosclerosis increased from 2 to 3 mo and from 3 to 4 mo. Inflammation (CD68) decreased and apoptosis (anti–cleaved-caspase 3 antibody) increased in aortic sinus slices measured as percentage of lesion by 4 mo. With increasing lesion stage, lesion inflammation decreased and lesion apoptosis increased. Aortic arch inflammation (^{18}F-FDG uptake) did not differ over time and did not correlate with average lesion stage. However, aortic arch apoptosis (^{99m}Tc-rhAnnexin V-128) increased significantly by 4 mo and correlated with average lesion stage. There were no differences between the treatment subgroups (^{18}F-FDG, ^{99m}Tc-rhAnnexin V-128, or no radiotracer). **Conclusion:** The temporal pattern of development of inflammation and apoptosis differ during the development of atherosclerosis in ApoE$^{-/-}$ mice treated with low-dose radiation. Advanced lesions are characterized by increased apoptosis and either less or similar amounts of inflammation, shown on immunohistochemistry and autoradiography. Treatment with radiotracers had no significant effects on extent of atherosclerosis, inflammation, or apoptosis.

Key Words: atherosclerosis; autoradiography; ^{99m}Tc-rhAnnexin V-128; ^{18}F-fluorodeoxyglucose

J Nucl Med 2016; 57:1784–1791
DOI: 10.2967/jnumed.116.172346

The relationship between radiation exposure and atherosclerosis is appreciated but not well defined. The long-term risk of cardiovascular disease in Japanese atomic bomb survivors (*1*) and medically exposed populations (*2*) is increased after exposure to moderate radiation doses. A very low dose of approximately 30 mSv is associated with increased atherosclerosis in occupationally exposed workers (*3*). Systematic reviews were inconclusive, with no clear evidence for increased cardiovascular risk with low-dose radiation (*4*).

Extrapolating the effects of high-dose to low-dose radiation may be misleading. Studies of aortic lesions in apolipoprotein E–deficient (ApoE$^{-/-}$) mice with single low-dose exposures of 25 and 50 mGy showed protective effects of low doses with a decrease in aortic lesions and both protective and adverse effects with high doses (*5*). Similar protective results were observed with low-dose radiation in ApoE$^{-/-}$ mice with reduced tumor protein p53 function (*6*). Low-dose radiation in ApoE$^{-/-}$ mice reduces plasma inflammatory markers, and larger doses produce a proinflammatory and prothrombotic response (*7*). Otherwise, the mechanisms resulting in the protective effects with low-dose radiation have not been explored.

Inflammation participates in the development of atherosclerosis and its complications, including plaque rupture (*8,9*). Plaque rupture is related to inflammation at the plaque edges with infiltration of macrophages, which overexpress matrix metalloproteinases (*10*) and undergo apoptosis (*11*). ^{18}F-FDG uptake identifies plaque inflammation due to increased glucose utilization by activated macrophages (*12*). Plaque apoptosis has been detected with ^{99m}Tc-labeled annexin V in animal models (*13,14*). In 25-wk-old ApoE$^{-/-}$ mice, both ^{18}F-FDG and ^{99m}Tc-labeled annexin V accumulated in plaque, with greater uptake of ^{99m}Tc-labeled annexin V in advanced plaques (*15*). However, little data exist describing the temporal pattern of the development of inflammation with ^{18}F-FDG and apoptosis with ^{99m}Tc-labeled annexin V imaging in ApoE$^{-/-}$ mice on a high-fat diet and particularly with a low-dose radiation model.

Received Jan. 13, 2016; revision accepted May 10, 2016.
For correspondence contact: Terrence Ruddy, University of Ottawa Heart Institute, H1220 - 40 Ruskin St., Ottawa, Ontario, Canada K1Y 4W7.
E-mail: truddy@ottawaheart.ca
Published online Jun. 15, 2016.

The radiation doses of ^{18}F-FDG and ^{99m}Tc-labeled annexin V used for imaging studies can result in large acute exposures to mice and are of a magnitude similar to that used for the low-dose radiation model (*16,17*). It is possible that this acute exposure may alter the atherosclerotic process or the effects of low-dose radiation.

The primary objective was to evaluate the extent of atherosclerosis, inflammation with ^{18}F-FDG, and apoptosis with ^{99m}Tc-rhAnnexin V-128 in ApoE$^{-/-}$ mice receiving single low-dose radiation with assessment at 2, 3, and 4 mo of age. The secondary objective was to compare the effects of radiation from the radiotracers with no radiotracer in the same low-dose radiation model of atherosclerosis on the study endpoints.

MATERIALS AND METHODS

Animals

Female barrier-raised ApoE$^{-/-}$ mice (B6.129P2-ApoE$^{tmL/Unc}$/J, strain no. 002052) obtained at 3 wk of age from Jackson Laboratory were group-housed as specific-pathogen-free mice at Chalk River Laboratories. The mice were fed a Western, high-fat diet (TD.10885; Harlan Laboratories) at 1 mo of age with free access to water and food.

The mice were exposed to ^{60}Co γ-radiation at a low dose of 25 mGy at 2 mo of age using 1 mGy/min as a single dose from an open beam source (GammaBeam 150; Canadian Nuclear Laboratories). The 60 mice were divided into 3 groups of 20 mice. The mice were transferred to the University of Ottawa Heart Institute (UOHI) animal care facility at 3 time points for euthanasia, autoradiography, and tissue analysis. One group was transferred the day after irradiation (2-mo group). The other 2 groups were maintained for a further 1 (3-mo group) or 2 mo (4-mo group) on the high-fat diet and then transferred. The mice were observed for 1 wk at the UOHI before the experimental procedures were started. Each group of 20 was divided into 3 subgroups of no radiotracer, ^{18}F-FDG for inflammation imaging, and ^{99m}Tc-rhAnnexin V-128 for apoptosis imaging.

All housing, handling, and experimental procedures were in strict accordance with the guidelines of Canadian Council on Animal Care and with approval of the Animal Care Committees of the UOHI and Canadian Nuclear Laboratories.

Autoradiography, Tissue Collection, En Face, and Oil Red O Imaging

For mice receiving radiotracer, either ^{18}F-FDG (74 MBq [2 mCi]) was administered as an intraperitoneal injection with the mice awake or ^{99m}Tc-rhAnnexin V-128 (55.5 MBq [1.5 mCi]) was injected by tail vein with the mice sedated under light anesthesia with 1%–2% isoflurane. ^{18}F-FDG was produced by the Radiochemistry Laboratory at the UOHI with radiochemical purity of over 98%. ^{99m}Tc-rhAnnexin V-128 was prepared from an Annexin V-128 kit for ^{99m}Tc labeling (Advanced Accelerator Applications International). Approximately 740 MBq (20 mCi) of $^{99m}TcO_4^-$ in 2 mL of saline were added to the kit vial containing the lyophilized rhAnnexin V-128 formulation. The vial was rotated on a roller at room temperature for 90 min. The product was analyzed by a size-exclusion high-pressure liquid chromatography column (BioSEP SEC-S2000 column, 300 × 7.8 mm, 5 μm, 150 Å; Phenomenex). The mobile phase was a solution with 20 mM NaH_2PO and 300 mM

TABLE 1
Effect of Treatment and Time on Extent of Atherosclerosis

Parameter	Time after radiation		
	2 mo	3 mo	4 mo
En face (% aorta)			
No radiotracer	5.79 ± 1.91	14.84 ± 2.33*	23.02 ± 4.16†,‡
^{18}F-FDG	4.25 ± 1.58	14.16 ± 2.89*	26.96 ± 5.74†,‡
^{99m}Tc-rhAnnexin V-128	5.29 ± 2.51	15.45 ± 2.46*	23.37 ± 2.56†,‡
Oil red O (% aorta)			
No radiotracer	8.26 ± 1.97	16.77 ± 2.09*	28.72 ± 4.72†,‡
^{18}F-FDG	4.83 ± 1.91	17.60 ± 2.44*	28.94 ± 4.23†,‡
^{99m}Tc-rhAnnexin V-128	8.13 ± 2.75	14.37 ± 3.77*	27.36 ± 5.26†,‡
Lesion area (mm^2)			
No radiotracer	0.059 ± 0.043	0.176 ± 0.120*	0.333 ± 0.153†,‡
^{18}F-FDG	0.048 ± 0.033	0.159 ± 0.120*	0.352 ± 0.164†,‡
^{99m}Tc-rhAnnexin V-128	0.059 ± 0.042	0.167 ± 0.128*	0.343 ± 0.091†,‡
Lesion severity			
No radiotracer	1.38 ± 0.42	2.10 ± 0.67*	2.97 ± 0.83†,‡
^{18}F-FDG	1.27 ± 0.27	2.08 ± 0.71*	3.03 ± 0.80†,‡
^{99m}Tc-rhAnnexin V-128	1.36 ± 0.47	1.99 ± 0.71*	3.11 ± 0.81†,‡

*$P < 0.01$ (2 vs. 3 mo).
†$P < 0.001$ (3 vs. 4 mo).
‡$P < 0.001$ (2 vs. 4 mo).
Data are mean ± SD.

NaCl at pH 6 and pumped through the high-pressure liquid chromatography at a flow rate of 1 mL/min. The retention time of the ^{99m}Tc-rhAnnexin V-128 signal was 9.1 min. The radiochemical purity was more than 85%.

Mice were euthanized in a CO_2 chamber with the gas delivered using a compressed gas cylinder with a pressure regulator and a flowmeter. Mice receiving radiotracer were euthanized 2–4 h after radiotracer injection. Mice were perfused using a peristaltic pump (Gilson Minipuls 2) with 20 mL of phosphate-buffered saline followed by 10 mL of 10% formalin via left ventricular cannulation. Perfusate was drained from a cut within the right atrium. The aorta was dissected from the heart at the base using a dissecting microscope after removal of surrounding fat and connective tissue. The weights of arch and descending aorta were recorded. After removal of adventitial tissue, the aorta was opened longitudinally, pinned onto a black wax surface using microneedles, imaged with autoradiography, and photographed (en face imaging). Lipid-rich intraluminal lesions were stained with Oil red O and photographed. The en face and Oil red O lesions were analyzed by 2 observers using Image Pro software (Media Cybernetics), and the extent of atherosclerosis was expressed as the percentage of the aorta (*18,19*).

The distributions of ^{18}F-FDG and ^{99m}Tc-rhAnnexin V-128 in aortic tissue were evaluated with digital autoradiography. En face specimens were immediately exposed to super-resolution phosphor screens. After an exposure time of 1 h for ^{18}F-FDG and 12 h for ^{99m}Tc-rhAnnexin V-128 at room temperature, the screens were scanned with a Cyclone Phosphor Imager (PerkinElmer) in a high-sensitivity autoradiography cassette (FisherBiotech). Images were analyzed using OptiQuant 5.0 software (Packard Instruments Co.) by drawing an aortic arch region of interest from the boundary between the aortic root and the ascending aorta to the same level on the

TABLE 2
Effect of Treatment and Time on Inflammation

Parameter	Time after radiation		
	2 mo	3 mo	4 mo
CD68			
% of lesion			
Section A			
No radiotracer	76.76 ± 11.03	51.86 ± 20.65*	38.28 ± 11.26†
^{18}F-FDG	77.25 ± 8.98	62.85 ± 12.24	42.50 ± 9.93†,‡
^{99m}Tc-rhAnnexin V-128	76.43 ± 13.29	54.80 ± 12.79	34.79 ± 5.37†
Section B			
No radiotracer	69.17 ± 10.51	55.89 ± 17.05	42.38 ± 14.46†
^{18}F-FDG	76.85 ± 11.63	66.24 ± 15.50*	45.81 ± 8.60†
^{99m}Tc-rhAnnexin V-128	79.06 ± 11.97	51.04 ± 11.89*	40.78 ± 11.37†
Section C			
No radiotracer	74.05 ± 8.31	53.93 ± 18.72	45.75 ± 14.04†,‡
^{18}F-FDG	68.44 ± 17.27	64.13 ± 14.49	53.42 ± 15.14†,‡
^{99m}Tc-rhAnnexin V-128	76.06 ± 14.48	58.53 ± 7.22	36.59 ± 10.30†
Area (mm^2)			
Section A			
No radiotracer	0.075 ± 0.017	0.135 ± 0.040*	0.153 ± 0.053†
^{18}F-FDG	0.053 ± 0.022	0.170 ± 0.055*	0.180 ± 0.032†
^{99m}Tc-rhAnnexin V-128	0.056 ± 0.037	0.110 ± 0.038	0.161 ± 0.026‡
Section B			
No radiotracer	0.053 ± 0.013	0.110 ± 0.032*	0.146 ± 0.043†
^{18}F-FDG	0.035 ± 0.016	0.127 ± 0.042*	0.162 ± 0.050†
^{99m}Tc-rhAnnexin V-128	0.052 ± 0.037	0.098 ± 0.045	0.139 ± 0.036†
Section C			
No radiotracer	0.032 ± 0.013	0.069 ± 0.026*	0.124 ± 0.034†
^{18}F-FDG	0.018 ± 0.012	0.079 ± 0.034*	0.134 ± 0.054†,‡
^{99m}Tc-rhAnnexin V-128	0.044 ± 0.031	0.077 ± 0.048	0.097 ± 0.022

*$P < 0.01$ (2 vs. 3 mo).
†$P < 0.001$ (2 vs. 4 mo).
‡$P < 0.001$ (3 vs 4 mo).
Data are mean ± SD.

TABLE 3
Effect of Treatment and Time on Apoptosis

Parameter	Time after radiation		
	2 mo	3 mo	4 mo
Apoptosis			
% of lesion			
Section A			
No radiotracer	0.021 ± 0.067	0.506 ± 0.456	1.881 ± 0.463†,‡
^{18}F-FDG	0.003 ± 0.004	0.484 ± 0.464	1.971 ± 0.658†,‡
^{99m}Tc-rhAnnexin V-128	0.011 ± 0.023	0.896 ± 0.515*	2.197 ± 0.542†,‡
Section B			
No radiotracer	0.003 ± 0.007	0.451 ± 0.506	1.377 ± 0.516†,‡
^{18}F-FDG	0.004 ± 0.009	0.306 ± 0.480	1.395 ± 0.609†,‡
^{99m}Tc-rhAnnexin V-128	0.016 ± 0.023	0.590 ± 0.375	1.594 ± 0.526†,‡
Section C			
No radiotracer	0.007 ± 0.022	0.222 ± 0.280	1.302 ± 0.550†,‡
^{18}F-FDG	0.001 ± 0.004	0.044 ± 0.066	1.407 ± 0.422†,‡
^{99m}Tc-rhAnnexin V-128	0.018 ± 0.018	0.389 ± 0.285	1.416 ± 0.312†,‡
Area (mm^2)			
Section A			
No radiotracer	0.000 ± 0.000	0.001 ± 0.001	0.009 ± 0.003†,‡
^{18}F-FDG	0.000 ± 0.000	0.001 ± 0.001	0.010 ± 0.005†,‡
^{99m}Tc-rhAnnexin V-128	0.000 ± 0.000	0.002 ± 0.002	0.010 ± 0.002†,‡
Section B			
No radiotracer	0.000 ± 0.000	0.001 ± 0.001	0.004 ± 0.002†,‡
^{18}F-FDG	0.000 ± 0.000	0.001 ± 0.001	0.005 ± 0.002†,‡
^{99m}Tc-rhAnnexin V-128	0.000 ± 0.000	0.001 ± 0.001	0.006 ± 0.002†,‡
Section C			
No radiotracer	0.00 ± 0.00	0.001 ± 0.001	0.003 ± 0.002†,‡
^{18}F-FDG	0.00 ± 0.00	0.000 ± 0.000	0.004 ± 0.003†,‡
^{99m}Tc-rhAnnexin V-128	0.00 ± 0.00	0.001 ± 0.000	0.004 ± 0.001†,‡

*$P < 0.01$ (2 vs. 3 mo).
†$P < 0.001$ (3 vs. 4 mo).
‡$P < 0.001$ (2 vs. 4 mo).
Data are mean ± SD.

descending aorta. Counts in digital light units and surface areas in mm^2 were measured. Values of digital light units were converted to activity in μCi using a set of calibration standards with known activities, which were exposed and scanned on the same screen used for the aorta samples and corrected for decay. The percentage injected dose was calculated from dividing the activity (μCi) of the sample by the injected activity. Activity density in percentage injected dose/mm^2 was calculated and normalized by animal body weight.

Histology and Immunohistochemistry

Quantification of the atherosclerotic lesions in tissue sections of the aortic root was performed as previously described (*20*). The aortic sinus was dissected from the heart, embedded in optimal-cutting-temperature medium, and frozen at −20°C. The sinus was aligned so that the 3 aortic valves would appear simultaneously in the section. Sections were 10-μm thick and separated by 100 μm. Sections were stained with Sudan IV. Lesion area was defined as intimal tissue within the internal elastic lamina. Analysis began with the first section of tissue that was lacking remnants of the aortic valves defining the boundary between the aortic sinus and the descending artery. The lesion cross-sectional area in each section was measured in 5 sections using Image-Pro Plus (Media Cybernetics) software with images obtained with a digital camera (Infinity 2; Lumenera Corp.) mounted to a compound microscope. The lesion area for each mouse was calculated as the average of 5 sections and measured by 2 independent observers with results averaged.

Lesions were classified into 5 stages identifying their severity in the range of 1–5 (less severe to more severe) based on the staining pattern and morphologic features of the 5 serial sections by 2 independent observers with results averaged. The human lesion classification format (*21,22*) was used. Stages 1–3 indicate early stages of severity

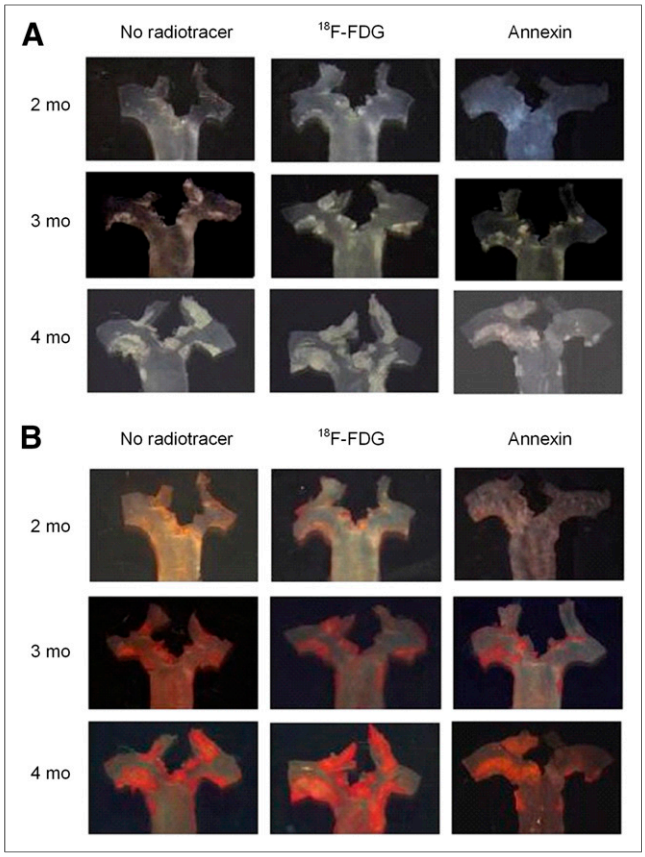

FIGURE 1. Extent of aortic atherosclerosis shown by en face (A) and Oil red O images (B). Extent increased over time (2, 3, and 4 mo) but did not differ with treatment (no radiotracer, ^{18}F-FDG, and ^{99m}Tc-rhAnnexin V-128).

containing predominantly foam cells, whereas stage 4 and 5 lesions are characterized by necrotic core with or without a fibrous cap.

Inflammation was detected with CD68 antibody immunostaining of the first 3 serial sections (sections a, b, and c). After the sections for internal hydrogen peroxides and background antibody binding were blocked, sections were incubated in rat antimouse CD68 primary antibody at the concentration of 1:500 in a nonpermeablizing condition followed by incubation with a biotinylated secondary antibody against rat IgG protein and visualized by peroxidase staining (Vectastain Elite ABC kit; Vector Laboratories) and a DAB solution (3,3′-diaminobenzidine tetrahydrochloride, Sigma D5905; Sigma-Aldrich Canada Co.). Finally, sections were counterstained with hematoxylin. The lesion area staining positive for macrophages was quantified using Image-Pro software, and percentage of CD68-positive area from the entire lesion area was calculated.

Active or cleaved caspase 3, an early marker of apoptosis, was used to identify cells undergoing apoptosis within the lesion area. Once sections were blocked for endogenous peroxidase, avidin/biotin, and general background staining, sections were incubated with anti–cleaved-caspase 3 antibody (Cell Signaling Technology) in a 1:300 dilution in the presence of permeablizing reagent. This antibody exclusively detects endogenous levels of caspase-3 protein only when cleaved at Asp175. Secondary staining was performed in the presence of signal stain boost secondary antibody (Cell Signaling Technology) followed by chromogenic staining by peroxidase substrate. Finally, hematoxylin counterstaining was performed. The same 3 sections that were analyzed for inflammation staining were studied for positivity. The lesion area staining positive for caspase-3 was quantified using Image-Pro software, and percentage of cleaved caspase 3–positive area from the entire lesion area was calculated.

Statistical Analysis

Data are reported as mean ± SD. Two-way ANOVA followed by pairwise comparisons using Tukey correction was used to evaluate the 2 factors of time (2, 3, and 4 mo) and treatment (no radiotracer, ^{18}F-FDG, or ^{99m}Tc-rhAnnexin V-128). One-way ANOVA followed by pairwise comparisons with Tukey correction was used to compare multiple groups determined by lesion stage or time in months. Because atherosclerosis may vary between aortic slices with greater disease in the proximal slices (*23*), the extent of treatment and time on inflammation and apoptosis was compared on a slice-by-slice basis. The Pearson correlation coefficient was used to measure the extent of linear dependence between lesion stage versus inflammation and apoptosis. Statistical analysis was performed using GraphPad Prism

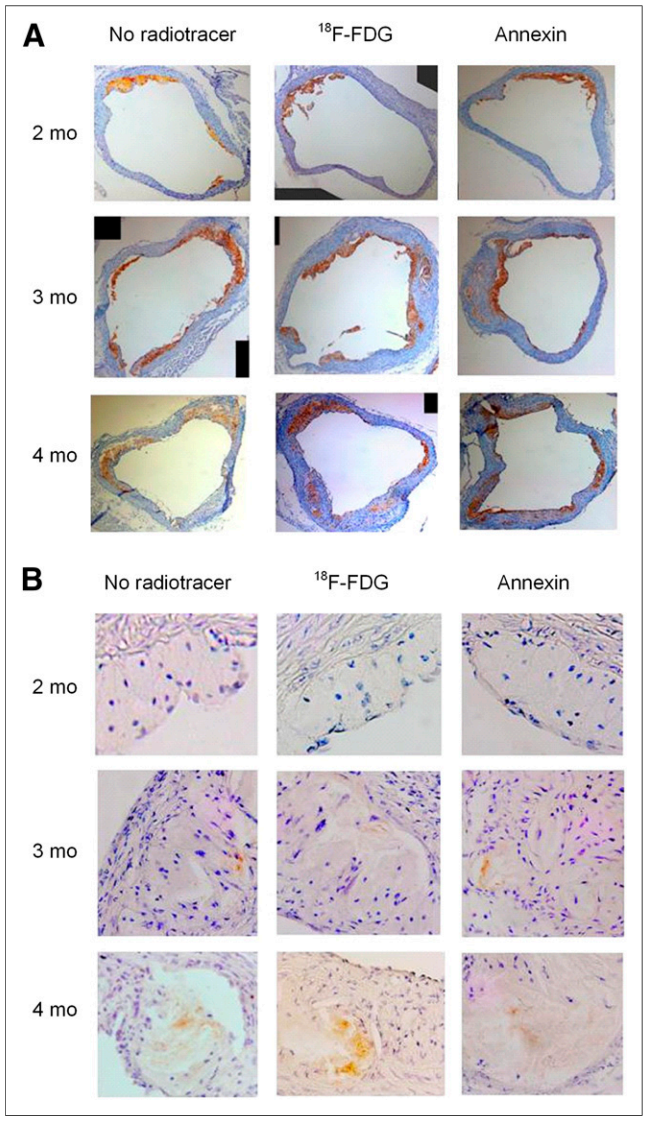

FIGURE 2. Inflammation shown by anti-CD68 antibody (A) and apoptosis by caspase 3 staining (B) in aortic sinus slices. Inflammation and apoptosis increased over time but did not differ with treatment (no radiotracer, ^{18}F-FDG, and ^{99m}Tc-rhAnnexin V-128).

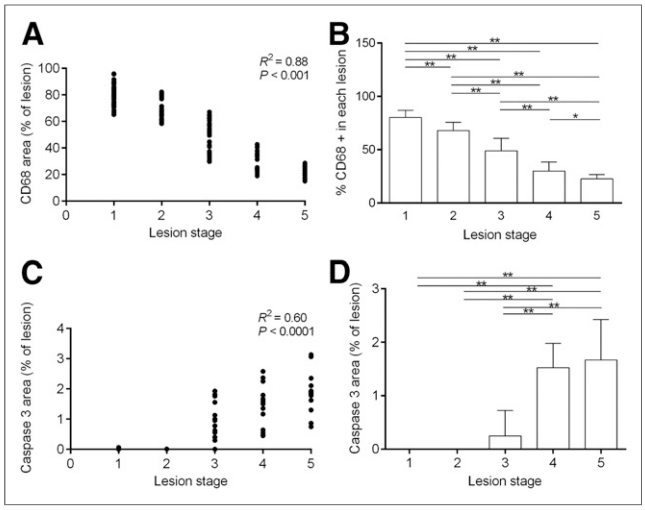

FIGURE 3. Inflammation and apoptosis related to lesion stage in aortic sinus slices. Inflammation (A and B) decreased with increasing stages. Apoptosis (C and D) increased with stages 4 and 5. $^*P < 0.01$. $^{**}P < 0.0001$

(version 6.01; GraphPad Software). A P value of less than 0.05 was considered statistically significant.

RESULTS

Effect of Treatment (No Radiotracer, ^{18}F-FDG, or ^{99m}Tc-rhAnnexin V-128) and Time on Atherosclerosis, Inflammation, and Apoptosis

Atherosclerosis was evaluated with en face and Oil red O imaging as percentage of aorta, lesion area, and lesion severity (Table 1). Inflammation was measured with anti-CD68 antibody (Table 2) and apoptosis with caspase 3 staining (Table 3), both as percentage of lesion and area. All of these parameters differed with time (2, 3, or 4 mo) ($P < 0.0001$). However, the same parameters were not affected by exposure to radiotracer (^{18}F-FDG or ^{99m}Tc-rhAnnexin V-128) with no significant interaction. Pairwise analysis showed significant changes with time (2 vs. 3 vs. 4 mo) for each treatment group but no significant differences between treatment groups at each time point. Thus, treatment had no significant effects on extent of atherosclerosis, inflammation, or apoptosis.

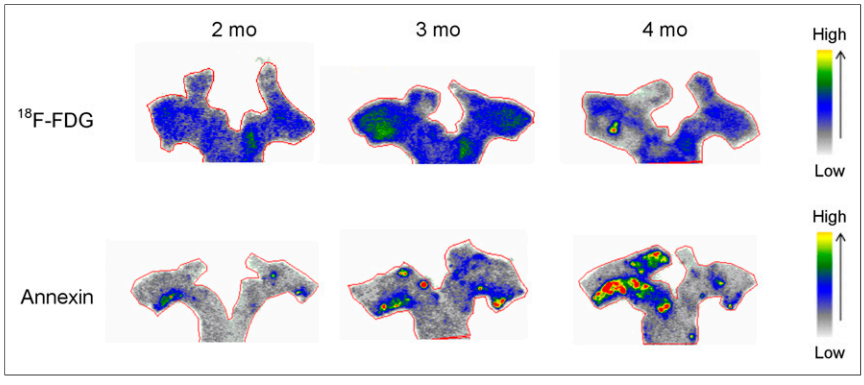

FIGURE 4. Autoradiographs of aortic arch showing inflammation (^{18}F-FDG) and apoptosis (^{99m}Tc-rhAnnexin V-128). Inflammation was similar, and apoptosis increased over time.

Temporal Pattern of Development of Atherosclerosis

The extent of atherosclerosis increased significantly from 2 to 3 mo and 3 to 4 mo (Table 1; Fig. 1). Inflammation (CD68) decreased as percentage of lesion by 4 mo and increased as area by 4 mo (Table 2; Fig. 2A). Apoptosis (caspase 3 antibody) increased as percentage of lesion and as area by 4 mo (Table 3; Fig. 2B).

Inflammation as percentage of lesion decreased with increasing lesion stage ($R^2 = 0.88$, $P < 0.001$), with a significant decrease in inflammation with each increase in stage (Figs. 3A and 3B). Apoptosis as percentage of lesion increased with lesion stage ($R^2 = 0.60$, $P < 0.001$), with absent or near-absent presence in lesions of stages 1–3 and significant increases in stages 4 and 5 lesions (Figs. 3C and 3D).

Autoradiography with ^{18}F-FDG and ^{99m}Tc-rhAnnexin V-128

Aortic arch uptake of ^{18}F-FDG did not differ between the time points of 2, 3, and 4 mo (Figs. 4 and 5A). No significant correlation was found between aortic arch uptake of ^{18}F-FDG and average lesion stage (Fig. 6A).

Aortic arch uptake of ^{99m}Tc-rhAnnexin V-128 differed between time points, with significantly greater uptake at 4 mo than at 2 and 3 mo (Figs. 4 and 5B). Aortic arch uptake of ^{99m}Tc-rhAnnexin V-128 correlated well with average lesion stage ($R^2 = 0.48$, $P = 0001$, Fig. 6B).

DISCUSSION

The principal finding was a difference in the temporal pattern of inflammation and apoptosis during the development of atherosclerosis in ApoE$^{-/-}$ mice treated with low-dose radiation. As lesion histologic area increased by 6-fold by 4 mo, lesion inflammation with anti-CD68 antibody immunostaining increased by 2- to 3-fold as area in mm^2 but decreased relatively as percentage of lesion (due to the greater relative increase in lesion area). Lesion apoptosis measured with anti–cleaved-caspase 3 antibody immunostaining increased to a greater degree by 5- to 10-fold as area in mm^2 and increased relatively as percentage of lesion by 4 mo. Advanced lesions were characterized by increased apoptosis and either less or similar amounts of inflammation, shown on immunohistochemistry and autoradiography. The second finding was no significant effects of treatment with radiotracers on extent of atherosclerosis, inflammation, or apoptosis.

The autoradiographic data measured at 2, 3, and 4 mo showed no difference in ^{18}F-FDG uptake and a significant increase in ^{99m}Tc-rhAnnexin V-128 at 4 mo. The lack of temporal change in ^{18}F-FDG uptake may be due to the increase in inflammation extent being relatively diluted by the increasing lesion size as shown by the anti-CD68 antibody immunostaining histologic data. The ^{99m}Tc-rhAnnexin V-128 autoradiographic and immunohistochemistry data were concordant, with both showing increased apoptosis at 4 mo, possibly in part due to the greater increases seen in apoptosis. Zhao et al. showed significantly higher aortic arch uptake levels of ^{18}F-FDG and ^{99m}Tc-annexin V5 in ApoE$^{-/-}$ mice aged 18 versus 10 wk (*24*). The differences in ^{18}F-FDG results may be related to differences in methods.

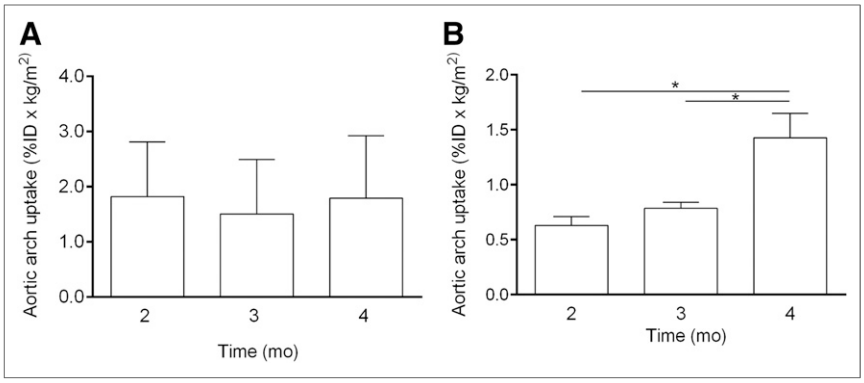

FIGURE 5. Aortic arch uptake measured from autoradiographs of inflammation (A, ^{18}F-FDG) and apoptosis (B, ^{99m}Tc-rhAnnexin V-128). ID = injected dose. *$P < 0.0001$

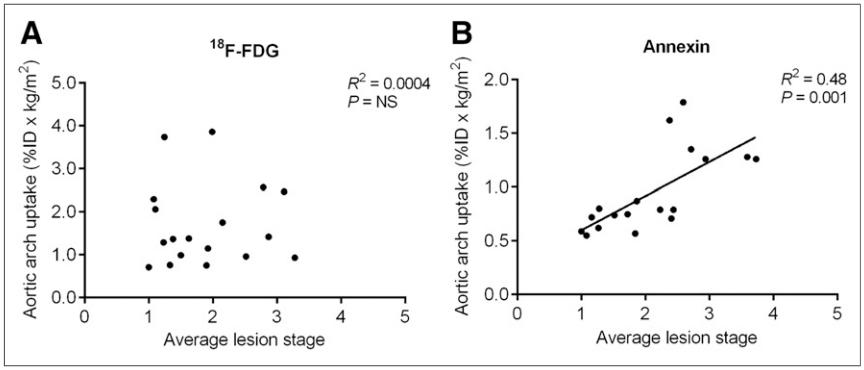

FIGURE 6. Relationship of aortic arch uptake of ^{18}F-FDG (A) and ^{99m}Tc-rhAnnexin V-128 (B) to aortic average lesion stage. ID = injected dose. NS = not significant.

Our results showed a decrease in inflammation as percentage of lesion with increasing lesion stage and an increase in apoptosis as percentage of lesion in stage 4 and 5 lesions. Zhao et al. found greater autoradiographic uptake of ^{18}F-FDG and ^{99m}Tc-annexin V5 in advanced lesions classified as early or late by Oil red O staining for lipid content in ApoE$^{-/-}$ mice (*15*). Oil red O staining identifies lipid content, which is only in part related to lesion stage. Our differing ^{18}F-FDG results may be due to differences in methods (lesion vs. aortic arch uptake, Oil red O uptake on imaging vs. Sudan IV lesion classification, low-dose radiation model). Our ^{99m}Tc-annexin V5 results were similar. Kolodgie et al. imaged apoptosis with ^{99m}Tc-annexin V5 in a rabbit balloon-injury model of atherosclerosis and showed greater uptake of ^{99m}Tc-annexin V5 in advanced stage 4 lesions than early stage 2–3 lesions (*13*), similar to our results.

ApoE$^{-/-}$ mice receiving low-dose radiation exposures of 25–50 mGy at 2 mo have less aortic atherosclerosis measured at 5 mo of age (*5*). The estimated doses for a 30-g mouse would be 66 mGy for ^{99m}Tc-rhAnnexin V-128 (55.5 MBq [1.5 mCi]) and 800 mGy for ^{18}F-FDG (74 MBq [2 mCi]) (*16,17*). Thus, the exposure for small-animal SPECT or PET imaging is similar and may alter atherosclerosis. However, our results showed no measurable difference in the extent of atherosclerosis, inflammation, and apoptosis for the comparison of the subgroups (^{18}F-FDG, ^{99m}Tc-rhAnnexin V-128, and no radiotracer). This is reassuring for ongoing research with molecular imaging and this animal model.

CONCLUSION

The temporal patterns of development of inflammation and apoptosis differ during the development of atherosclerosis in ApoE$^{-/-}$ mice treated with low-dose radiation. Lesion inflammation decreased and apoptosis increased by 4 mo. Advanced lesions were characterized by increased apoptosis and either less or similar amounts of inflammation, shown with immunohistochemistry and autoradiography. Treatment with radiotracers had no significant effects on extent of atherosclerosis, inflammation, or apoptosis.

DISCLOSURE

The costs of publication of this article were defrayed in part by the payment of page charges. Therefore, and solely to indicate this fact, this article is hereby marked "advertisement" in accordance with 18 USC section 1734. This study was funded by a research grant to the University of Ottawa Heart Institute from the Canadian Nuclear Laboratories, previously Atomic Energy of Canada Limited. Michelle Bugden, Heather M. Wyatt, Nicholas D. Priest, and Ronald E. Mitchel are employees of Canadian Nuclear Laboratories. No other potential conflict of interest relevant to this article was reported.

ACKNOWLEDGMENTS

We thank Laurie Bennet and Lyanne Fuller for their assistance with the preparation of this manuscript.

REFERENCES

1. Sakata R, Grant EJ, Ozasa K. Long term follow-up of atomic bomb survivors. *Maturitas.* 2012;72:99–103.
2. Galper SL, Yu JB, Mauch PM, et al. Clinically significant cardiac disease in patients with Hodgkin lymphoma treated with mediastinal irradiation. *Blood.* 2011;117:412–418.
3. Howe GR, Zablotska LB, Fix JJ, Egel J, Buchanan J. Analysis of the mortality experience amongst U.S. nuclear power industry workers after chronic low-dose exposure to ionizing radiation. *Radiat Res.* 2004;162:517–526.
4. McGale P, Darby SC. Low doses of ionizing radiation and circulatory diseases: a systematic review of the published epidemiological evidence. *Radiat Res.* 2005;163:247–257.
5. Mitchel REJ, Hasu M, Bugden M, et al. Low-dose radiation exposure and atherosclerosis in ApoE$^{-/-}$ mice. *Radiat Res.* 2011;175:665–676.
6. Mitchel REJ, Hasu M, Bugden M, et al. Low-dose radiation exposure and protection against atherosclerosis in ApoE$^{-/-}$ mice: the influence of P53 heterozygosity. *Radiat Res.* 2013;179:190–199.
7. Libby P. Inflammation in atherosclerosis. *Arterioscler Thromb Vasc Biol.* 2012;32:2045–2051.
8. Mathias D, Mitchel REJ, Barclay M, et al. Low-dose irradiation affects expression of inflammatory markers in the heart of ApoE$^{-/-}$ mice. *PLoS One.* 2015;10:e0119661.
9. Davies MJ, Thomas A. Thrombosis and acute coronary artery lesions in sudden cardiac ischemic death. *N Engl J Med.* 1984;310:1137–1140.
10. Shah PK, Falk E, Badimon JJ, et al. Human monocyte-derived macrophages induce collagen breakdown in fibrous caps of atherosclerotic plaques. *Circulation.* 1995;92:1565–1569.

11. Björkerud S, Björkerud B. Apoptosis is abundant in human atherosclerotic lesions, especially in inflammatory cells (macrophages and T cells), and may contribute to the accumulation of gruel and plaque instability. *Am J Pathol.* 1996;149:367–380.
12. Tawakol A, Migrino RQ, Hoffman U, et al. Noninvasive in vivo measurement of vascular inflammation with F-18 fluorodeoxyglucose positron emission tomography. *J Nucl Cardiol.* 2005;12:294–301.
13. Kolodgie FD, Petrov A, Virmani R, et al. Targeting of apoptotic macrophages and experimental atheroma with radiolabeled annexin V: a technique with potential for noninvasive imaging of vulnerable plaque. *Circulation.* 2003;108: 3134–3139.
14. Tekabe Y, Li Q, Luma L, et al. Noninvasive monitoring the biology of atherosclerotic plaque development with radiolabeled annexin V and matrix metalloproteinase inhibitor in spontaneous atherosclerotic mice. *J Nucl Cardiol.* 2010;17:1073–1081.
15. Zhao Y, Kuge Y, Zhao S, et al. Comparison of ^{99m}Tc-annexin A5 with ^{18}F-FDG for the detection of atherosclerosis in ApoE−/− mice. *Eur J Nucl Med Mol Imaging.* 2007;34:1747–1755.
16. Funk T, Sun M, Hasegawa BH. Radiation dose estimate in small animal SPECT and PET. *Med Phys.* 2004;31:2680–2686.
17. Taschereau R, Chatziioannou AF. Monte Carlo simulations of absorbed dose in a mouse phantom from 18-fluorine compounds. *Med Phys.* 2007;34:1026–1036.
18. Rayner K, Chen YX, McNulty M, et al. Extracellular release of the atheroprotective heat shock protein 27 is mediated by estrogen and competitively inhibits acLDL binding to scavenger receptor-A. *Circ Res.* 2008;103:133–141.
19. Chen YX, Ma X, Whitman S, O'Brien ER. Novel antiinflammatory vascular benefits of systemic and stent-based delivery of ethylisopropylamiloride. *Circulation.* 2004;110:3721–3726.
20. Daugherty A, Whitman SC. Quantification of atherosclerosis in mice. *Methods Mol Biol.* 2003;209:293–309.
21. Stary HC, Chandler AB, Glagov S, et al. A definition of initial, fatty streak and intermediate lesions of atherosclerosis. *Circulation.* 1994;89:2462–2478.
22. Stary HC, Chandler AB, Dinsmore RE, et al. A definition of advanced types of atherosclerotic lesions and a histological classification of atherosclerosis. *Circulation.* 1995;92:1355–1374.
23. Purcell-Huynh DA, Farese RV, Johnson DF, et al. Transgenic mice expressing high levels of human apolipoprotein B develop severe atherosclerotic lesions in response to a high-fat diet. *J Clin Invest.* 1995;95:2246–2257.
24. Zhao Y, Kuge Y, Zhao S, et al. Prolonged high-fat feeding enhances aortic ^{18}F-FDG and ^{99m}Tc-annexin A5 uptake in apolipoprotein E-deficient and wild-type C57BL/6J mice. *J Nucl Med.* 2008;49:1707–1714.